A design of a surface-doped Yb:YAG slab laser with high power and high efficiency

Jiao Liu (刘 娇)[1,2], Yang Liu (刘 洋)[1,2], Xiaojun Tang (唐晓军)[1,2], Chao Wang (王 超)[1,2,*], Lei Liu (刘 磊)[1,2], Lu Chen (陈 露)[1,2], Ning Li (李 宁)[1,2], Ke Wang (王 柯)[1,2], Xingbo Liang (梁兴波)[1,2], Kunpeng Lü (吕坤鹏)[1,2], Xue Yang (杨 雪)[1,2], Hong Zhao (赵 鸿)[1,2], and Nianjiang Chen (陈念江)[1,2]

[1]*Institute of North Optics and Electronics, Beijing 100015, China*
[2]*Science and Technology on Solid-State Laser Laboratory, Beijing 100015, China*
**Corresponding author: bitmissliu@sina.com*

Received June 27, 2018; accepted August 16, 2018; posted online September 14, 2018

We demonstrate a high-efficiency and high-power quasi-three-level laser based on a trapezoidal composite slab architecture with a 270 μm-thick Yb-doping surface. The design of a surface-doped slab architecture, temperature effects, laser oscillator model, and laser oscillator experiments with a surface-doped slab as a laser host medium have been presented. By theoretical calculation, the temperature rise in the surface-doped slab is only one seventh of that in the bulk-doped slab at the same maximum pump power of 30 kW. Finally, in the laser oscillator experiments, an output energy of 21.6 J is obtained when the pump energy is 48 J with a repetition rate of 5 Hz and a pulse width of 1 ms. The optical-optical efficiency is 45%.

OCIS codes: 140.3380, 140.3460, 140.3580, 140.3615.
doi: 10.3788/COL201816.101401.

High-power solid-state lasers have widespread applications because they are efficient, compact, robust, and with good beam equality[1]. In addition, with the achievement of high-power laser diodes with a high beam quality, there has been an increased interest in the quasi-three-level laser host medium during the past 10 years[2–4]. Compared to a four-level laser medium, Yb:YAG, as a quasi-three-level laser medium, has attracted a great amount of attention for its advantages of higher photon efficiency, the associated lower thermal loading, no excited state absorption, no concentration quenching, and no upconversion, which paves the way for high-power solid-state lasers[5,6].

To date, there are many architectures of the Yb:YAG medium that have been demonstrated for high-power laser systems, including the thin-disk and slab structure, etc. In 2014, Schad *et al.*[7] reported near fundamental mode operation of Yb-doped thin-disk lasers. The output power of 4 kW with optical-optical efficiency of 56% has been achieved by pumping at 969 nm. The beam equality factor is $M^2 < 1.4$. Because of face cooling, the thin-disk lasers have a less transversal temperature gradient and the phase distortions transversal to the direction of the beam propagation. However, In order to be absorbed well, the pump structures are usually complicated. Another high-power gain medium structure, the zigzag slab structure is of great interest for eliminating thermal gradient induced lensing in the thickness direction and minimizing stress gradient induced birefringence. In 2016, Chen *et al.*[8] demonstrated a composite Yb:YAG crystal slab with three doped and two undoped segments with symmetrical configuration. For an 0.8 kW seed input, a maximum output power of 3.54 kW is obtained at 6.7 kW of pump power, with the optical conversion efficiency of 41% and the highest slope efficiency of 59%. In addition, a Yb:YAG planar waveguide laser with an output power of 16.1 kW was reported[9,10]. The architecture leverages a slab-based master oscillator power amplifier (MOPA) architecture based on a planar waveguide amplifier. The technical objectives for this effort are to demonstrate >25 kW output with an excellent beam quality and an electrical to optical efficiency >30%.

In this Letter, we demonstrate a high-power and high-efficiency surface-doped Yb:YAG slab structure to more efficiently remove the waste heat generated by the pump source. The design of a surface-doped slab gain medium is established, and the properties of the slab, such as the temperature effects and the output characteristics, are analyzed theoretically. Finally, the laser oscillator experiments are demonstrated with a surface-doped slab as the laser host medium.

The surface-doped Yb:YAG slab geometry is shown in Fig. 1. A trapezoidal surface-doped slab structure is demonstrated to remove waste heat more efficiently. Different from the normal bulk Yb-doping slab, only one of surfaces of the slab is Yb-doped. The doped surface is mounted on a copper water-cooled heat sink and the other undoped one is directly in contact with the air.

The laser beam follows a zigzag path between two surfaces by multiple total internal reflections (TIRs). A coordinate system is defined as follows. The x direction is along the thickness, y is along the width, and z is along the length. The full width is W, the full thickness is H, and the full length is L.

Before we can proceed with an analysis of the laser performance, the slab temperature distribution is required. Therefore, we need to solve the thermal conduction

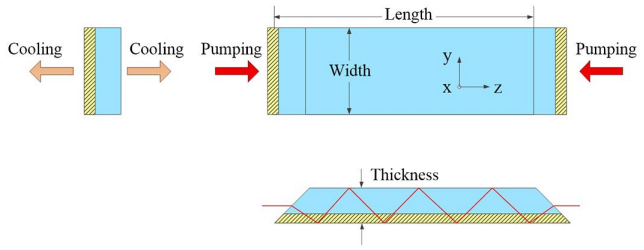

Fig. 1. Orthographic drawing of a surface-doped slab.

equations with thermal boundary conditions at different surfaces[11]. In the steady state, the thermal conduction equation is

$$\nabla^2 T(x,y,z) = \frac{-Q(x,y,z)}{k(x,y,z)}, \tag{1}$$

where $Q(x,y,z)$ is the heat generated per unit volume in the slab, which is assumed to be zero except in the doped region, $k(x,y,z)$ is the thermal conductivity, and T is the temperature, which is assumed to be a quadratic function of x in the doped region and a linear function in the undoped region along the x axis followed by

$$T = \begin{cases} ax+b & x_0 \le x \le H-h+x_0, \\ cx^2+d & x_0-h \le x \le x_0, \end{cases} \tag{2}$$

with the thermal boundary conditions:

$$k_1 \frac{\mathrm{d}T}{\mathrm{d}x}\bigg|_{x=x_0} = k_2 \frac{\mathrm{d}T}{\mathrm{d}x}\bigg|_{x=x_0}, \tag{3}$$

$$k_1 \frac{\mathrm{d}T}{\mathrm{d}x}\bigg|_{x=x_0-h} = -\lambda_1 (T_1 - T|_{x=x_0-h}), \tag{4}$$

$$k_2 \frac{\mathrm{d}T}{\mathrm{d}x}\bigg|_{x=x_0-h+H} = -\lambda_2 (T_2 - T|_{x=x_0-h+H}), \tag{5}$$

$$T_1|_{x=x_0} = T_2|_{x=x_0}, \tag{6}$$

where λ_1 and λ_2 are the surface heat transfer coefficients, T_1 and T_2 are the coolant temperatures, the highest temperature appears at $x = x_0$, and the thickness of the doped region is h. Then it is an algebraic problem to solve Eq. (1) through Eq. (6).

According to the above model, the temperature gradients in the slab are simulated and the results are shown in Fig. 2.

From Fig. 2(a), we see that due to the structure of surface-doped slab, the temperature along the direction of thickness is asymmetrical and the highest temperature of about 38.5°C exists at $x = x_0 \approx 0.27$ mm near the surface between the doping region and undoping region [the red line in Fig. 2(a)], when the pump power is 30 kW. Figure 2(b) shows that the temperature along the length has a saddle shape, which is low at the center and high

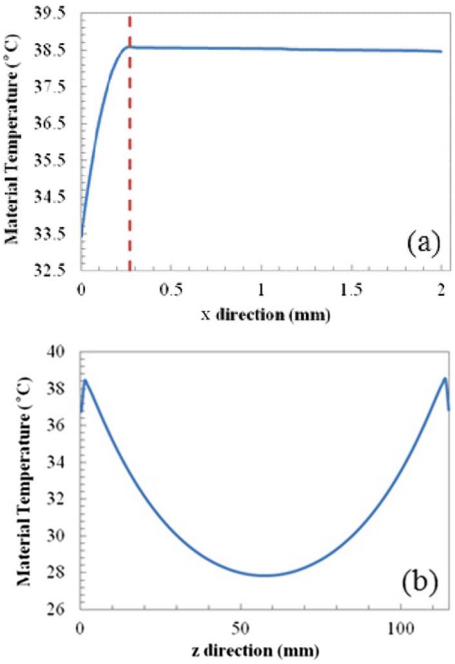

Fig. 2. (a) Temperature distribution along the thickness at $y = 14$, $z = 1.25$; (b) temperature distribution along the length at $x = 0.27$, $y = 14$. The slab has outside dimensions of 28 mm width by 113.2 mm length by 2 mm thickness, consisting of a 0.27 mm-thickness Yb^{3+}-doping surface with a concentration of 2 at. %, and the slab is double-end-pumped with a pump power of 30 kW at 940 nm.

near the ends because of the cooling on the bottom face of the slab. The highest temperature appears at the distance of 1.25 mm from the end with a pump power of 30 kW.

The highest temperatures of the surface-doped slab and the normal bulk-doped slab with the same size and same absorption are also compared. The simulated results of the highest temperature in the slabs are shown in Fig. 3.

From Fig. 3, we can see the advantages of the surface-doped slab concept. Compared with the temperature of 38°C of the surface-doped slab, the highest temperature of the bulk-doped slab is about 164°C when the pump power is 30 kW. The temperature increase in the slab is only

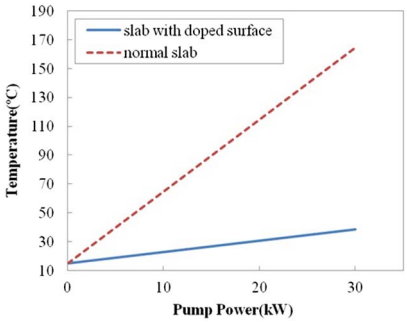

Fig. 3. Comparison of the highest temperature of the surface-doped slab and the normal bulk-doped slab over a wide pump power range.

one seventh of that in the normal slab. For a uniformly pumped slab of infinite extent, the stress is found to be[12]

$$\sigma = \frac{\beta E}{1-v}\Delta T, \tag{7}$$

where β is thermal expansion coefficient, E is Young's modulus, v is Poisson's ratio, $\Delta T = T - T_{\text{ave}}$ is the temperature distribution that characterizes a change in temperature, and T_{ave} is the average temperature. The maximum stress or stress fracture limit that can be tolerated by the laser host material YAG prior to fracture is usually $(1.3\text{–}2.6) \times 10^3$ kg/cm^2.

We now present a model of a surface-doped Yb:YAG slab laser. The schematic diagram of a laser beam path in a slab is shown in Fig. 4.

As shown in Fig. 4, the incidence angle of the laser beam matches the condition of total internal reflection. Based on geometrical optics, the times of the laser total internal reflection in the slab are followed by

$$n = \frac{L}{H}\tan\left[\gamma + \arcsin\left(\frac{\sin\theta}{n_{\text{YAG}}}\right)\right], \tag{8}$$

where θ is the angle of incidence on the end face, γ is the chamfer angle of end faces, and n_{YAG} is the refractive index of the slab. Thus, the effective gain length l_{eff} can be defined as

$$l_{\text{eff}} = h \cdot \left\{\frac{L}{H}\cdot\frac{1}{\sin\left[\gamma + \arcsin\left(\frac{\sin\theta}{n_{\text{YAG}}}\right)\right]} + \frac{1}{\cos\left[\gamma + \arcsin\left(\frac{\sin\theta}{n_{\text{YAG}}}\right)\right]}\right\}, \tag{9}$$

where h is the thickness of doping area. The structure of the slab must match the odd times of laser total reflection. In addition, the absorption efficiency is not less than 95%, which can be written as

$$\eta_{\text{abs}} = \frac{1 - e^{-\sigma_a \Delta n_{\text{eff}} l_{\text{eff}}}}{1 - R_p e^{-\sigma_a \Delta n_{\text{eff}} l_{\text{eff}}}} > 95\%, \tag{10}$$

where σ_a is the absorption cross section, and Δn_{eff} is given by

$$\begin{aligned}\Delta n_{\text{eff}} &= f_a^p n_d - (f_a^p + f_b^p) n_U \\ &= \frac{f_a^p f^l - f_a^l f^p}{f^l} n_d - \frac{f^p}{f^l}\frac{1}{2\beta\sigma_e l_{\text{eff}}}\ln\left[\frac{1}{R_{\text{OC}}(1-\delta)^2}\right],\end{aligned} \tag{11}$$

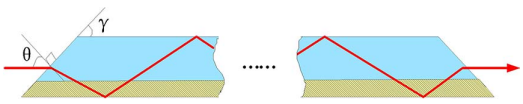

Fig. 4. Schematic diagram of the laser beam path in the slab.

where n_d is the dopant concentration; δ is the one-way cavity loss; R_{OC} is the laser output coupler reflectivity; β is a zigzag overlap factor that measures the amount of beam overlap in the zigzag path varying from 1 to 2; σ_e is the stimulated emission cross section; f_a^l, f_b^l are the Boltzmann population fractions for the lower and upper laser levels; f_a^p, f_b^p are the Boltzmann population fractions for the lower and upper pump levels; and $f^l = f_a^l + f_b^l$, $f^p = f_a^p + f_b^p$. Figure 5 shows the Stark level spectrum of Yb:YAG.

The value for the upper manifold population n_U is defined by

$$n_U = \frac{1}{2f^l\beta\sigma_e l_{\text{eff}}}\ln\left[\frac{1}{R_{\text{OC}}(1-\delta)^2}\right] + \frac{f_a^l}{f^l}n_d. \tag{12}$$

The laser output power P_{out} of a continuous wave (CW) quasi-three-level laser oscillator is a function of the pump power[13,14],

$$P_{\text{out}} = \eta_{\text{slope}}(\eta_{\text{abs}} P_p - P_{\text{th}}), \tag{13}$$

where P_p is the pump power. The laser slope efficiency η_{slope} and the threshold pump power required for lasing P_{th} are calculated by

$$\eta_{\text{slope}} = \eta_{\text{mode}}\frac{\nu_L}{\nu_P}\frac{1 - R_{\text{OC}}}{1 - R_{\text{OC}} + \sqrt{R_{\text{OC}}}\left(\frac{1}{1-\delta} + \delta - 1\right)}, \tag{14}$$

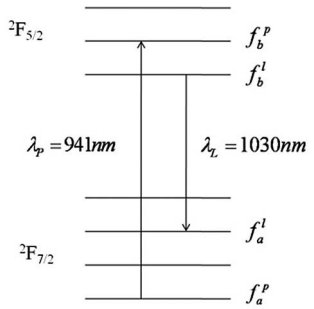

Fig. 5. Energy level scheme of the Yb:YAG laser system. The Boltzmann occupation factors of the Stark levels coupled by the pump radiation are denoted by f_a^p and f_b^p. The Boltzmann occupation factors of the Stark levels coupled by the laser emission are denoted by f_a^l and f_b^l.

$$P_{\text{th}} = \frac{h\nu_P}{\tau} hWLn_U, \tag{15}$$

where η_{mode} is the mode-fill efficiency, ν_L is the laser transition frequency, ν_P is the pump transition frequency, and τ is the excited manifold storage lifetime.

Based on the above analysis, the curves of the absorbed efficiency and the output power with different thicknesses of the doped region are shown in Fig. 6.

Figure 6 clearly shows that, as the thickness of the doped region increases to 0.27 mm, the absorbed efficiency and the output power dramatically rise up to 95% and 16 kW, respectively. When the thickness of the doped region increases from 0.27 mm to 0.7 mm, the absorbed efficiency varies slightly from 95% to 99%, but the output power drastically drops from 16 kW to 12 kW. Thus, taking into account both the high output power and high absorbed efficiency, the slab is designed with following parameters. The slab has outside dimensions of 28 mm width by 113.2 mm length by 2 mm height, consisting of a 0.27 mm-thickness Yb^{3+}-doping surface with a concentration of 2 at. %. The incidence angle on the end face of pump light is about 22°.

We apply the discussed parameters to Eq. (9)–Eq. (15) and calculate the laser output power and optical-optical efficiency for the double-end-pumped surface-doped Yb:YAG slab laser. The calculated results are shown in Fig. 7.

By using the designed surface-doped Yb:YAG laser, a maximum output power of 16.0 kW can be obtained with an optical-optical efficiency of 53.3% and a slope efficiency of 60.2% at a pump power of 30 kW. At the same time, according to the analysis of the previous section, the maximum thermal stress of about 754 kg/cm^2 occurs at a distance of 1.25 mm from the ends. The safety factor is 0.58, which is within the range of the stress safety, so it can work steadily for a long time.

The experimental configuration of the double-end-pumped surface-doped Yb:YAG slab laser system is shown in Fig. 8. The slab has outside dimensions of 28 mm width by 113.2 mm length by 2 mm height, consisting of a 0.27 mm-thickness Yb^{3+}-doping surface with a concentration of 2 at. %. The two end faces of the slab are 45°-cut and antireflection coated at 103 nm and 940 nm. The two sides of the slab are roughened to suppress the amplified spontaneous emission (ASE) and parasitic oscillation. The doped surface is mounted on a copper water-cooled heat sink and the other undoped one is in direct contact with air.

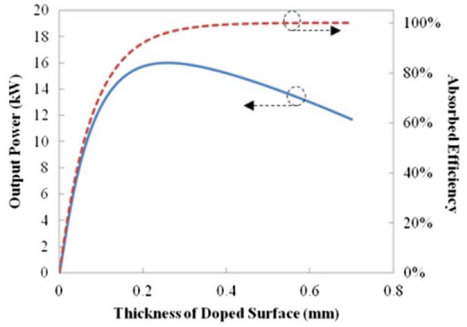

Fig. 6. Curves of the absorbed efficiency and the output power with different thicknesses of the doped region, when the pump power is 30 kW and the output coupler reflectivity R is 0.75.

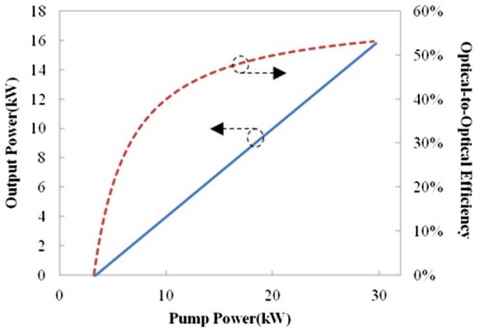

Fig. 7. Predicted laser output power and optical-optical conversion efficiency against the pump power with an output coupler reflectivity R of 0.75. The pump power at the lasing threshold is about 3.4 kW and the slope efficiency is 60.2%.

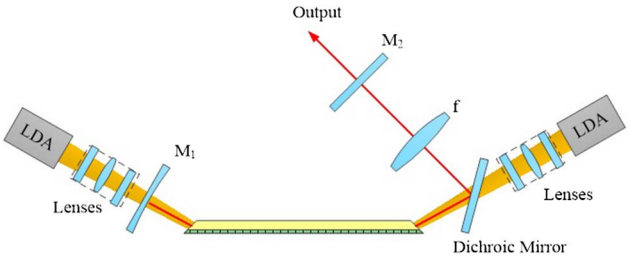

Fig. 8. Schematic of the experimental setup.

The curvature radius of the mirror M_1 is 2 m, with one face antireflection coated at 940 nm and the other one high-reflection coated at 940 nm and 1030 nm. The output coupler reflectivity R is 0.75. The focal length of the lens f is 300 mm.

The system uses two diode laser stacks emitting at 940 nm, with a maximum output pulse energy of 24 J. The pump beam shaping system is comprised of three cylindrical lenses. The incidence angle on the end face of pump light is about 22°.

The pump pulse at a repetition rate of 5 Hz with a width of 1 ms is used. The laser oscillator output energy and optical-optical efficiency are plotted in Fig. 9.

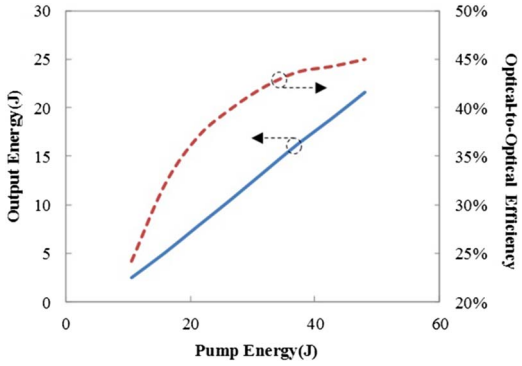

Fig. 9. Laser oscillator performance for a 48 J double-end-pumped surface-doped Yb:YAG slab laser.

It can be seen that the output energy increases linearly with the increase of pump energy. In addition, the optical-optical efficiency increases with the increase of pump energy and gradually tends to saturation. The output energy of 21.6 J is obtained with a pump energy of 48 J, corresponding to 21.6 kW of output peak power and 48 kW of pump peak power. The optical-optical efficiency is 45%.

The surface-doped slab geometry offers a robust and scalable laser design. A thermal analysis of the laser host material studied is presented which indicates that the surface-doped slab has greater heat dissipation ability than counterparts. The temperature increase in the surface-doped slab is only one seventh of that in the normal slab at the same pump power of 30 kW. An output power of 16 kW can be obtained with an optical-optical efficiency of 53.3% and slope efficiency of 60.2%. The threshold of pump power is about 3434 W. In the experiments, an output energy of 21.6 J is obtained with a repetition rate of 5 Hz and a pulse width of 1 ms under the pump energy of 48 J. The optical-optical efficiency is 45%, and a slope efficiency is 50.9%. The measured threshold of the pump peak power is about 3544 W, which is a little higher than the theoretical results. The optimization of the pump uniformity and the improved laser design will be researched in our future work.

This project is funded by the Science and Technology on Solid-State Laser Laboratory.

References

1. J. Liu, L. Ge, L. Feng, H. Jiang, H. Su, T. Zhou, J. Wang, Q. Gao, and J. Li, Chin. Opt. Lett. **14**, 051404 (2016).
2. H. W. Bruesselbach, D. S. Sumida, R. A. Reeder, and R. W. Byren, IEEE J. Sel. Top. Quantum Electron. **3**, 105 (1997).
3. C. Bibeau, R. J. Beach, S. C. Mitchell, M. A. Emanuel, J. A. Skidmore, C. A. Ebbers, S. B. Sutton, and K. S. Jancaitis, IEEE J. Quantum Electron. **34**, 2010 (1998).
4. W. F. Krupke, IEEE J. Sel. Top. Quantum Electron. **6**, 1287 (2000).
5. W. F. Krupke and L. L. Chase, Opt. Quantum Electron. **22**, S1 (1989).
6. A. Giesen, H. Hugel, A. Voss, K. Witting, U. Brauch, and H. Opower, Appl. Phys. B **58**, 365 (1994).
7. S. S. Schad, V. Kuhn, T. Gottwald, V. Negoita, A. Killi, and K. Wallmeroth, Proc. SPIE **8959**, 89590U (2014).
8. X. Chen, L. Xu, H. Hu, T. Zhou, Y. Sun, and H. Jiang, Opt. Express **24**, 24517 (2016).
9. T. Clatterbuck and D. Mordaunt, Proc. SPIE **8381**, 83810W (2012).
10. D. Filgas, D. Rockwell, and K. Spariosu, Raytheon Tech. Today **1**, 9 (2008).
11. T. S. Rutherford, W. M. Tulloch, E. K. Gustafson, R. L. Byer, and T. S. Rutherford, IEEE J. Quantum Electron. **36**, 205 (2000).
12. J. Eggleston, T. J. Kane, K. Kuhn, and J. Unternahrer, IEEE J. Quantum Electron. **20**, 289 (1984).
13. R. J. Beach, Opt. Commun. **123**, 385 (1996).
14. P. Peterson, A. Gavrielides, and P. M. Sharma, Opt. Commun. **109**, 282 (1994).